

A SINGLE DEGENERATE PROGENITOR MODEL FOR TYPE Ia SUPERNOVAE HIGHLY EXCEEDING THE CHANDRASEKHAR MASS LIMIT

IZUMI HACHISU

Department of Earth Science and Astronomy, College of Arts and Sciences, University of Tokyo, Komaba 3-8-1, Meguro-ku, Tokyo 153-8902, Japan

MARIKO KATO

Department of Astronomy, Keio University, Hiyoshi 4-1-1, Kouhoku-ku, Yokohama 223-8521, Japan

HIDEYUKI SAIO

Astronomical Institute, Graduate School of Science, Tohoku University, Sendai 980-8578, Japan

AND

KEN'ICHI NOMOTO

Institute for the Physics and Mathematics of the Universe, University of Tokyo, Kashiwa, Chiba 277-8583, Japan

accepted on 12th September 2011; to appear in the Astrophysical Journal

ABSTRACT

Recent observations of Type Ia supernovae (SNe Ia) suggest that some of the progenitor white dwarfs (WDs) had masses up to 2.4–2.8 M_{\odot} , highly exceeding the Chandrasekhar mass limit. We present a new single degenerate (SD) model for SN Ia progenitors, in which the WD mass possibly reaches 2.3–2.7 M_{\odot} . Three binary evolution processes are incorporated; optically thick winds from mass-accreting WDs, mass-stripping from the binary companion star by the WD winds, and WDs being supported by differential rotation. The WD mass can increase by accretion up to 2.3 (2.7) M_{\odot} from the initial value of 1.1 (1.2) M_{\odot} , being consistent with high luminosity SNe Ia such as SN 2003fg, SN 2006gz, SN 2007if, and SN 2009dc. There are three characteristic mass ranges of exploding WDs. In an extreme massive case, differentially rotating WDs explode as an SN Ia soon after the WD mass exceeds 2.4 M_{\odot} because of a secular instability at $T/|W| \sim 0.14$. For a mid mass range of $M_{\text{WD}} = 1.5\text{--}2.4 M_{\odot}$, it takes some time (spinning-down time) until carbon is ignited to induce an SN Ia explosion after the WD mass has reached maximum, because it needs a loss or redistribution of angular momentum. For a lower mass case of rigidly rotating WDs, $M_{\text{WD}} = 1.38\text{--}1.5 M_{\odot}$, the spinning-down time depends on the timescale of angular momentum loss from the WD. The difference in the spinning-down time may produce the “prompt” and “tardy” components. We also suggest the very bright super-Chandrasekhar mass SNe Ia are born in a low metallicity environment.

Subject headings: binaries: close — stars: winds, outflows — supernovae: individual (SN 2003fg, SN 2007if, SN 2009dc) — white dwarfs

1. INTRODUCTION

Type Ia supernovae (SNe Ia) play important roles in astrophysics, e.g., standard candles in cosmological distance and main production sites of iron-group elements. However, the nature of SN Ia progenitors is not fully understood yet (e.g., Niemeyer & Hillebrandt 2004; Nomoto et al. 2000). It has been widely accepted that SNe Ia are explosions of carbon-oxygen (C+O) white dwarfs (WDs). The observed features of SNe Ia are better explained by the Chandrasekhar mass model rather than the sub-Chandrasekhar mass model. It is not clear, however, how the WD mass gets close enough to the Chandrasekhar mass¹ for carbon ignition; i.e., whether the WD accretes H/He-rich matter from its binary companion [single degenerate (SD) scenario], or two C+O WDs merge [double degenerate (DD) scenario].

Recent observations of several very bright SNe Ia suggest that their progenitor WDs might have super-Chandrasekhar

masses of up to 2.4–2.8 M_{\odot} (e.g., Hicken et al. 2007; Howell et al. 2006; Scalzo et al. 2010; Silverman et al. 2011; Taubenberger et al. 2011; Yamanaka et al. 2009). Super-Chandrasekhar mass of the progenitors of SNe Ia was first reported by Howell et al. (2006) on SN 2003fg ($\sim 2.1 M_{\odot}$ C+O WD with $1.29 \pm 0.07 M_{\odot}$ ^{56}Ni). More candidates of super-Chandrasekhar mass progenitors were added to the list, i.e., SN 2006gz, SN 2007if, and SN 2009dc. Hillebrandt et al. (2007) suggested a possibility that SN 2003fg is an aspherical explosion of a Chandrasekhar mass WD. However, based on their recent spectropolarimetric observation of SN 2009dc which shows little continuum polarization of < 0.3 Tanaka et al. (2010) concluded that a very large asphericity was not likely to occur at the explosion of SN 2009dc. Moreover, the very bright SN 2007if require a $2.4 \pm 0.2 M_{\odot}$ progenitor C+O WD with $1.6 \pm 0.1 M_{\odot}$ ^{56}Ni (Scalzo et al. 2010) and SN 2009dc also demands $\gtrsim 2.0 M_{\odot}$ progenitor C+O WD with $1.4\text{--}1.7 M_{\odot}$ ^{56}Ni (Silverman et al. 2011) or $\sim 2.8 M_{\odot}$ C+O WD with $\sim 1.8 M_{\odot}$ ^{56}Ni (Taubenberger et al. 2011). Such a large WD mass, highly exceeding M_{Ch} , could challenge both the DD and SD scenarios. Some authors suggest a DD merger scenario for these super-Chandrasekhar mass SNe Ia (e.g.,

hachisu@ea.c.u-tokyo.ac.jp
mariko@educ.cc.keio.ac.jp
saio@astr.tohoku.ac.jp
nomoto@astron.s.u-tokyo.ac.jp

¹ Hereafter we use the Chandrasekhar mass $M_{\text{Ch}} = 1.46(Y_e/0.5)^2 M_{\odot}$ (e.g., Chandrasekhar 1939) for a *non-rotating* WD with electron mole number Y_e .

Scalzo et al. 2010; Silverman et al. 2011), mainly because the existing SD scenario provides only $M_{\text{WD}} \lesssim 1.8 M_{\odot}$ (e.g., Chen & Li 2009; Liu et al. 2010).

As for theoretical explosion models of super-Chandrasekhar mass WDs, Steinmetz et al. (1992) performed simulations of pure detonation models and found that almost all the matter is burned into iron group elements. Their results could not explain the observed intermediate mass elements seen in the spectra of SNe Ia. Recently, Pfannes et al. (2010) revised the simulations of pure detonation models based on Yoon & Langer’s (2005) super-Chandrasekhar mass models. They found that not all the WD matter is burned into iron group elements and some intermediate mass elements are synthesized in the outer low density region of the WD. The synthesized mass of nickel is large enough ($\sim 1.5 M_{\odot}$) to explain the super luminous SNe Ia such as SN 2009dc, which supports the super-Chandrasekhar mass models.

In the present paper, we show that such high WD masses are possibly explained by the SD scenario. There are three key binary evolution processes, i.e., optically thick winds from mass-accreting WDs (Hachisu et al. 1996), mass-stripping from the binary companion star by the WD winds (Hachisu et al. 2008a), and differential rotation which makes possible a WD more massive than the Chandrasekhar limit (Yoon & Langer 2004). The main difference of our SD model from the existing SD scenarios is that we take into account the effect of mass-stripping by the winds from mass-accreting WDs. We describe our basic assumptions and methods of binary evolutions in Section 2. Our numerical results are presented in Section 3. A possible binary evolution to our super-Chandrasekhar mass SNe Ia is suggested in Section 4. Discussion and concluding remarks follow in Sections 5 and 6, respectively.

2. MODELLING OF MASS-STRIPPING EFFECT AND BINARY EVOLUTION

First we briefly describe the method of our calculations for binary evolutions which is essentially the same as in Hachisu et al. (2008a) except that the evolution of the companion star is computed by a Henyey-type code. In a binary, the more massive (primary) component evolves to a red giant star (with a helium core) or an asymptotic giant branch (AGB) star (with a C+O core) and fills its Roche lobe. Dynamically unstable mass transfer begins from the primary to the secondary and forms a common envelope. After this first common envelope evolution, the separation shrinks and the primary becomes a helium star or a C+O WD. The helium star evolves to a C+O WD after a large part of helium is exhausted by core- and shell-helium-burning. Then the binary consists of a close pair of a C+O WD and a main-sequence (MS) star; from such a pair we start our calculations.

When the secondary expands to fill its Roche lobe, mass transfer begins from the secondary to the WD. If the secondary mass is more massive than the WD (precisely, when the mass ratio $q = M_{2,0}/M_{1,0} = M_{\text{MS},0}/M_{\text{WD},0} \gtrsim 0.8$), the mass transfer takes place on a thermal timescale. When the mass transfer rate exceeds the critical rate,

$$\dot{M}_{\text{cr}} = 6.68 \times 10^{-7} \left(\frac{M_{\text{WD}}}{M_{\odot}} - 0.445 \right) M_{\odot} \text{ yr}^{-1}, \quad (1)$$

optically thick winds blow from the WD (see Hachisu et al. 1996, 1999a,b; Nomoto et al. 2007, for more details).

The winds from the WD collide with the secondary and strips off its surface layer (Hachisu & Kato 2003a,b). This

mass-stripping effect attenuates the mass transfer from the secondary to the WD, thus preventing the formation of a common envelope even for a rather massive secondary. Thus the mass-stripping effect widens the donor mass range of SN Ia progenitors (e.g., Hachisu et al. 2008a,b).

We have incorporated the mass-stripping effect in the same way as in Hachisu et al. (2008a); i.e., the mass stripping rate \dot{M}_{strip} is related to the wind mass-loss rate \dot{M}_{wind} as

$$\dot{M}_{\text{strip}} = c_1 \dot{M}_{\text{wind}}, \quad (2)$$

with the factor c_1 defined as

$$c_1 \equiv \frac{\eta_{\text{eff}} \cdot g(q)}{\phi_{\text{L3}} - \phi_{\text{MS}}} \left(\frac{v^2 a}{2GM} \right), \quad (3)$$

where $M = M_{\text{WD}} + M_{\text{MS}}$, M_{WD} is the WD mass, M_{MS} is the main-sequence companion mass, a is the separation of the binary; ϕ_{L3} and ϕ_{MS} denote the Roche potential (normalized by GM/a) at the MS surface and the L3 point near the MS companion, respectively, i.e., $\phi_{\text{L3}} - \phi_{\text{MS}} \sim 0.3$; η_{eff} is the efficiency of conversion from kinetic energy to thermal energy by the shock, $g(q) \sim 0.025$ is the geometrical factor of the MS surface hit by the wind including the inclination (oblique shock) effect of the wind velocity against the companion’s surface (see Hachisu et al. 1999a, for more details on $g(q)$), and $q \equiv M_2/M_1 = M_{\text{MS}}/M_{\text{WD}}$ is the mass ratio. Here we modify equation (21) of Hachisu et al. (1999a) to include the effect of Roche lobe overflow from the L3 point. We assume $\eta_{\text{eff}} = 1$ in the present calculation. If the wind velocity is as fast as $4,000 \text{ km s}^{-1}$, we have $c_1 \sim 10$ as estimated by Hachisu & Kato (2003a). Hachisu & Kato (2003a,b) found best fit models at $c_1 = 1.5 - 10$ for RX J0513.9–6953 and at $c_1 = 7 - 8$ for V Sge, respectively. Here we adopt $c_1 = 1, 3$, and 10 to check the dependence of mass-stripping effect on the parameter c_1 .

The winds depend on the WD mass and metallicity (chemical composition). We have revised metallicity effects of WD winds (Figure 1 of Kobayashi et al. 1998). The results are shown in Figure 1. We did not find wind solutions but instead static envelope solutions for the “no winds” region. On the other hand, the “strong winds” region means that the wind velocity exceeds the escape velocity (see, e.g., Figure 4 of Kato & Hachisu 1994, for wind solutions). The velocity of the “weak winds” does not exceed the escape velocity. Winds are accelerated mainly by the peak of OPAL opacity due to iron lines while they are sometimes accelerated by a small opacity peak due to helium ionization for the relatively low metallicity region. Here we regard that stripping effect works only for strong winds. We have strong wind solutions (i.e., stripping effect) for $M_{\text{WD}} \gtrsim 0.6 M_{\odot}$ in the solar metallicity environment while for $M_{\text{WD}} \gtrsim 1.0 M_{\odot}$ in a low metallicity region of $Z = 0.001$ (Population II), and further for $M_{\text{WD}} \gtrsim 1.2 M_{\odot}$ in the much lower metallicity region of $[\text{Fe}/\text{H}] \lesssim -2$.

Mass accretion onto the WD spins it up because angular momentum is added to the WD (e.g., Langer et al. 2000; Paczynski 1991; Popham & Narayan 1991; Piersanti et al. 2003a,b; Uenishi et al. 2003). If the WD rotates rigidly, the mass of the WD can only slightly exceed the Chandrasekhar mass limit of no rotation, M_{Ch} . More massive WDs seem to be possible if they rotate differentially (e.g., Hachisu 1986). Based on simplified numerical calculations, Yoon & Langer (2004) showed that the WD can increase its mass beyond M_{Ch} when the accretion rate onto a WD is high enough ($\dot{M}_{\text{WD}} \gtrsim$

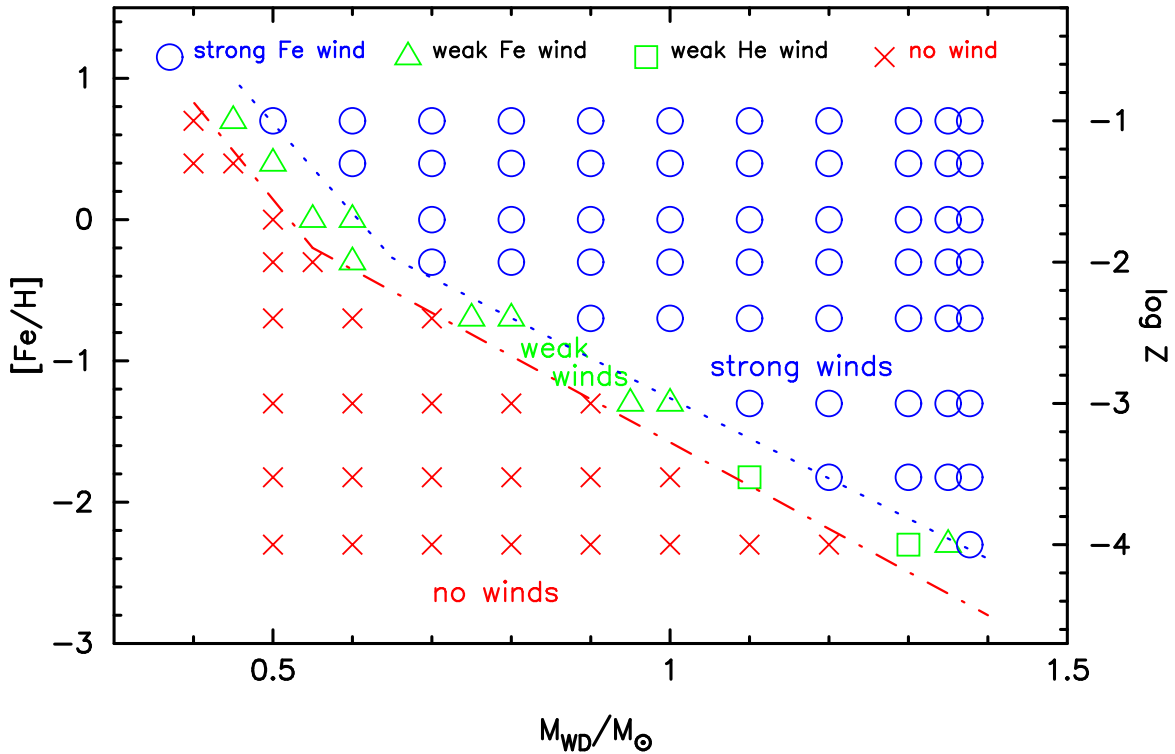


FIG. 1.— Wind region in the metallicity-WD mass diagram. Data are essentially the same as those in Figure 1 of Kobayashi et al. (1998) but a few points are revised. Each symbol shows as follows: strong winds (blue circles), weak winds (green triangles), both of which are driven by the OPAL peak at $\log T$ (K) = 5.2, weak winds (green squares) which are driven by the opacity peak due to helium ionization, and no winds (red crosses). “Strong winds” mean that the wind velocity exceeds the escape velocity while “weak winds” do not exceed. The blue dotted line shows a border of strong winds. The red dash-dotted line indicates a border of no winds. In the low metallicity region, strong winds blow only for very massive WDs (e.g., $M_{\text{WD}} \gtrsim 1.0 M_{\odot}$ for $[\text{Fe}/\text{H}] \lesssim -1$ and $M_{\text{WD}} \gtrsim 1.2 M_{\odot}$ for $[\text{Fe}/\text{H}] \lesssim -2$).

$10^{-7} M_{\odot} \text{ yr}^{-1}$) and the WD is differentially rotating. They showed that the gradient of rotational rate is kept around the critical value for the dynamical shear instability, because the timescale for the Eddington-Sweet meridional circulation is too long ($\sim 10^9$ yr) to redistribute angular momentum in the WD core, and that the differential rotation is strong enough for the WD mass to exceed M_{Ch} significantly.

In the present study, we simply assume that the WD is supported by differential rotation and its mass can increase without carbon being fused at the center as long as the mass accretion rate is higher than $3 \times 10^{-7} M_{\odot} \text{ yr}^{-1}$ ($\equiv \dot{M}_{\text{b}}$). We have adopted the limit by considering the fact that when $\dot{M}_{\text{WD}} < \dot{M}_{\text{b}}$ hydrogen shell-burning occurs intermittently and recurrent nova outbursts eject a large part of the hydrogen-rich envelope (e.g. Hachisu & Kato 2001). As a result, the net growth rate of the C+O core mass is reduced significantly so that the timescale of the angular momentum deposition on the WD would become comparable to the timescale for meridional circulation to re-distribute the angular momentum.

3. NUMERICAL RESULTS

3.1. Evolutions of WD+MS Systems

We have investigated evolutions of binaries which initially consist of a WD (primary) and a zero-age main-sequence (ZAMS) star, by calculating the evolutions of the secondary stars using a Henyey-type code (e.g., Saio et al. 1988). We have adopted a standard chemical composition of $(X, Z) = (0.70, 0.02)$ and used OPAL opacity tables (Iglesias & Rogers 1996). The mixing length is assumed to be 1.5 times the pressure scale height.

As the star evolves, the radius increases and eventually fills

its critical Roche lobe. Then, a mass transfer from the secondary to the primary WD begins. We have determined the rate of mass loss from the secondary, \dot{M}_2 , at each stage by requiring for the stellar radius to be equal to the mean radius of the Roche lobe. If $|\dot{M}_2|$ is smaller than the critical rate \dot{M}_{cr} given in Equation (1), all the matter from the secondary will be accreted onto the WD; i.e., $\dot{M}_1 = |\dot{M}_2|$. When the mass-accretion rate exceeds \dot{M}_{cr} , an optically thick wind blows from the WD. It causes mass-stripping from the secondary star as discussed in the previous section. Then, the systemic mass loss at a rate of $\dot{M}_{\text{wind}} + \dot{M}_{\text{strip}}$ occurs, which affects the evolution of the Roche lobe radius and hence \dot{M}_2 . During the evolution, \dot{M}_1 is given as $\min(\dot{M}_{\text{cr}}, |\dot{M}_2|)$ (see Hachisu et al. 1996, 1999a, 2008a, for details).

In the previous work (Hachisu et al. 2008a), we stopped the binary evolution at the epoch when the WD mass reached $1.38 M_{\odot}$, because we regarded that a WD explodes as an SN Ia at $M_{\text{WD}} = 1.38 M_{\odot}$ (Nomoto 1982a). In the present work, however, we further follow the binary evolution until the mass accretion rate of the primary WD decreases to $\dot{M}_1 = \dot{M}_{\text{b}} = 3 \times 10^{-7} M_{\odot} \text{ yr}^{-1}$, because the WD is expected to be supported by a strong differential rotation until then.

Although Equation (1) is based on the assumption of spherical symmetry (Nomoto et al. 2007), we consider it approximately applicable even for $M_{\text{WD}} > 1.38 M_{\odot}$ for the following reasons. Equation (1) is closely related to the local Eddington luminosity (and nuclear energy conversion rate per unit mass for hydrogen mass fraction, $X = 0.70$), which is mainly determined by the local opacity (peak) at a part with temperature of $\sim 2 \times 10^5$ K in the envelope. Since this layer is far from the

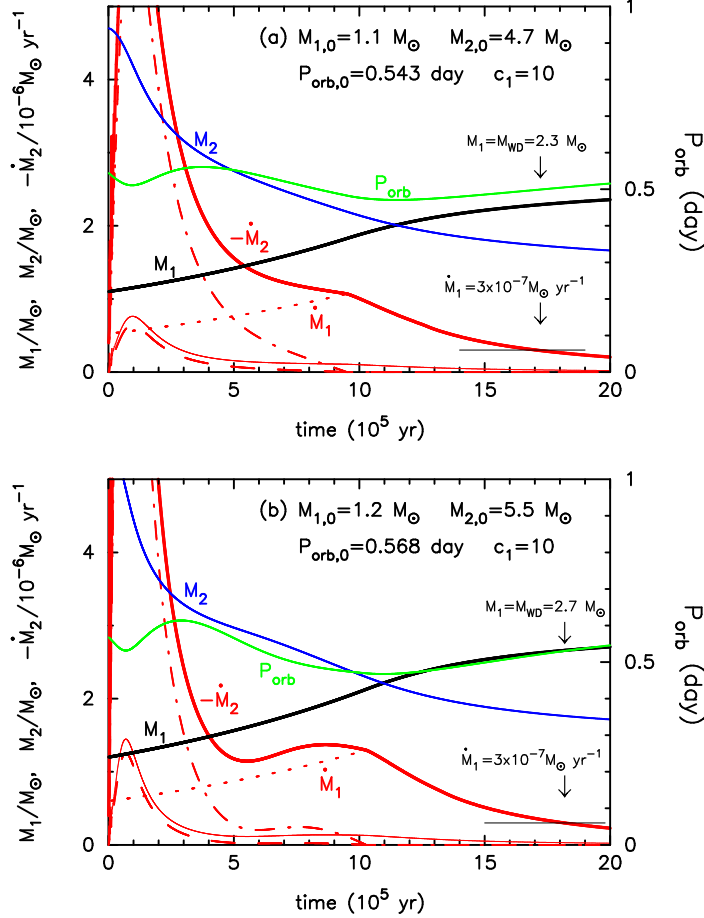


FIG. 2.— Binary evolutions of two WD+MS pairs: time starts when the mass transfer begins from the MS to the WD. (a) A WD of $M_{\text{WD},0} = 1.1 M_{\odot}$ and a MS star of $M_{\text{MS},0} = 4.7 M_{\odot}$ with the initial orbital period of $P_{\text{orb},0} = 0.543$ day (near ZAMS). The red thick solid line: the mass-loss rate from the MS companion, $-\dot{M}_2$. The red thin solid line: one tenth of the mass-loss rate, $-0.1\dot{M}_2$. The other solid lines denote the companion mass (blue), $M_2 \equiv M_{\text{MS}}$, the orbital period (green), P_{orb} , and the WD (primary) mass (black), $M_1 \equiv M_{\text{WD}}$, each symbol of which is attached to each line. The red dash-dotted line: stripping rate from the MS companion, \dot{M}_{strip} . The long red dashed line: the wind mass-loss rate from the WD, \dot{M}_{wind} . The red dotted line: the mass-increasing rate of the WD, $\dot{M}_1 \equiv \dot{M}_{\text{WD}}$, which is merged to the red solid line in the later time. The mass-loss rate, $-\dot{M}_2$, increases up to $6 \times 10^{-6} M_{\odot} \text{ yr}^{-1}$ and quickly drops to $1 \times 10^{-6} M_{\odot} \text{ yr}^{-1}$. Then, the optically thick wind stops and the mass-loss rate decreases to $-\dot{M}_2 = 3 \times 10^{-7} M_{\odot} \text{ yr}^{-1}$ at $t = 1.7 \times 10^6$ yr. At this time, the WD mass has increased to $M_1 = M_{\text{WD}} = 2.3 M_{\odot}$. (b) Same as (a) but for a pair of $1.2 M_{\odot}$ WD and $5.5 M_{\odot}$ MS with the initial orbital period of $P_{\text{orb},0} = 0.568$ day (near ZAMS). The mass-loss rate increases up to $-\dot{M}_2 = 1.5 \times 10^{-5} M_{\odot} \text{ yr}^{-1}$ and then quickly drops to $1 \times 10^{-6} M_{\odot} \text{ yr}^{-1}$. Then, the optically thick wind stops and the mass-loss rate decreases to $-\dot{M}_2 = 3 \times 10^{-7} M_{\odot} \text{ yr}^{-1}$ at $t = 1.8 \times 10^6$ yr. At this time, the WD mass has increased to $M_1 = M_{\text{WD}} = 2.7 M_{\odot}$.

C+O core surface (at the hydrogen shell burning region), the local Eddington luminosity should be insensitive to a rapid rotation of the C+O core.

We have followed binary evolutions for various sets of the initial parameters ($M_{\text{WD},0}, M_{2,0}, P_{\text{orb},0}$) and obtained maximum WD masses. In the first example, we set $c_1 = 10$ and assume $M_{\text{WD},0} = 1.1 M_{\odot}$, $M_{2,0} = 4.7 M_{\odot}$, and $P_{\text{orb},0} = 0.54$ day (the companion fills its Roche lobe after it slightly evolved off from ZAMS). The result is shown in Figure 2a. The mass-loss rate of the companion quickly increases up to $-\dot{M}_2 = 8 \times 10^{-6} M_{\odot} \text{ yr}^{-1}$ and then drops to $-\dot{M}_2 = 1 \times 10^{-6} M_{\odot} \text{ yr}^{-1}$ at $t = 10^6$ yr ($-\dot{M}_2$ is also plotted in the one tenth scale in the same figure by a red thin solid line). In the early phase of mass transfer, we have $-0.1\dot{M}_2 \approx \dot{M}_{\text{wind}}$ because $-\dot{M}_2 \approx \dot{M}_{\text{strip}}$ and $c_1 = 10$. As mass transfer rate decreases, the optically thick wind stops at $t \sim 1 \times 10^6$ yr, and the accretion rate \dot{M}_1 decreases to $3 \times 10^{-7} M_{\odot} \text{ yr}^{-1}$ at $t = 1.7 \times 10^6$ yr. The WD mass has increased to $2.3 M_{\odot}$ at this epoch. (Even if we adopt $\dot{M}_b = 1, 2, 3,$ and $4 \times 10^{-7} M_{\odot} \text{ yr}^{-1}$, the maximum WD mass does not change so much, i.e., 2.45, 2.36, 2.29, and $2.22 M_{\odot}$,

respectively. The dependence of the WD mass on the value of \dot{M}_b is very weak so that the adopted value itself is not essential for the results.)

In the second example, we assume a more massive binary with $c_1 = 10$, $M_{\text{WD},0} = 1.2 M_{\odot}$, $M_{2,0} = 5.5 M_{\odot}$, and $P_{\text{orb},0} = 0.57$ day (the companion fills its Roche lobe near ZAMS as in the first case). The result is shown in Figure 2b. The mass-loss rate of the companion increases up to $-\dot{M}_2 = 1.4 \times 10^{-5} M_{\odot} \text{ yr}^{-1}$ and then quickly decreases. The optically thick wind stops at almost the same time as in Figure 2a, $t = 1 \times 10^6$ yr, and afterward the mass transfer rate gradually decreased to $\dot{M}_1 = \dot{M}_b = 3 \times 10^{-7} M_{\odot} \text{ yr}^{-1}$ at $t = 1.8 \times 10^6$ yr. The WD mass has increased to $2.7 M_{\odot}$ at this epoch.

The third and fourth examples are for the binaries in which the companion fills its Roche lobe in a later phase, i.e., near the end of central hydrogen burning (Figure 3). The third example is for $c_1 = 10$, $M_{\text{WD},0} = 0.9 M_{\odot}$, $M_{2,0} = 3.5 M_{\odot}$, and $P_{\text{orb},0} = 1.38$ day. The result is shown in Figure 3a. The mass-loss rate of the companion increases up to $-\dot{M}_2 =$

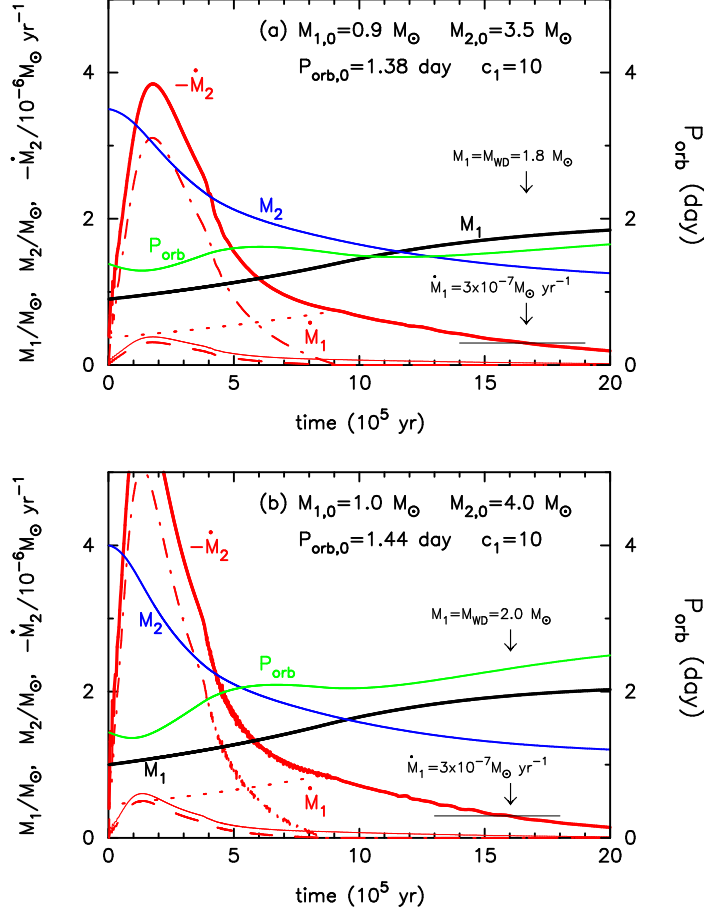


FIG. 3.— Same as Figure 2, but for the companion models near the end of central hydrogen-burning. (a) A WD of $M_{\text{WD},0} = 0.9 M_{\odot}$ and a MS of $M_{\text{MS},0} = 3.5 M_{\odot}$ with the initial orbital period of $P_{\text{orb},0} = 1.38$ day. The mass-loss rate from the companion decreases to $-\dot{M}_2 = 3 \times 10^{-7} M_{\odot} \text{ yr}^{-1}$ at $t = 1.67 \times 10^6$ yr. At this time, the WD mass has increased to $1.8 M_{\odot}$. (b) A WD of $M_{\text{WD},0} = 1.0 M_{\odot}$ and a MS of $M_{\text{MS},0} = 4.0 M_{\odot}$ with the initial orbital period of $P_{\text{orb},0} = 1.44$ day. The mass-loss rate decreases to $-\dot{M}_2 = 3 \times 10^{-7} M_{\odot} \text{ yr}^{-1}$ at $t = 1.59 \times 10^6$ yr. At this time, the WD mass has increased to $2.0 M_{\odot}$.

$3.8 \times 10^{-6} M_{\odot} \text{ yr}^{-1}$ and then quickly decreases. The optically thick wind stops at $t = 9 \times 10^5$ yr, and afterward the mass transfer rate is gradually decreasing to $\dot{M}_b = 3 \times 10^{-7} M_{\odot} \text{ yr}^{-1}$ at $t = 1.7 \times 10^6$ yr. The WD mass has increased to $1.8 M_{\odot}$ at this epoch.

In the fourth example, we have adopted $c_1 = 10$, $M_{\text{WD},0} = 1.0 M_{\odot}$, $M_{2,0} = 4.0 M_{\odot}$, and $P_{\text{orb},0} = 1.44$ day. The result is shown in Figure 3b. The mass-loss rate of the companion increases up to $-\dot{M}_2 = 6 \times 10^{-6} M_{\odot} \text{ yr}^{-1}$ and then quickly decreases. The optically thick wind stops at $t = 8 \times 10^5$ yr, and afterward the mass transfer rate is gradually decreasing to $\dot{M}_b = 3 \times 10^{-7} M_{\odot} \text{ yr}^{-1}$ at $t = 1.6 \times 10^6$ yr. The WD mass has increased to $2.0 M_{\odot}$ at this epoch.

In all the models, the mass-loss rate from the secondary, $-\dot{M}_2$, increases to $\gtrsim 3 \times 10^{-6} M_{\odot} \text{ yr}^{-1}$. If all the hydrogen-rich matter were converted into helium and then into carbon-oxygen and therefore accreted at the same rate as $-\dot{M}_2$, carbon burning would ignite off-center and the C+O core would be converted into O+Ne+Mg core (e.g., Kawai et al. 1988) so that the WD would not explode as an SN Ia. However, the net accretion rate to the WD is given as $|\dot{M}_2| - |\dot{M}_{\text{strip}}| - |\dot{M}_{\text{wind}}|$ ($= \dot{M}_1 \equiv \dot{M}_{\text{WD}}$ = the dotted lines in Figures 2 and 3), not exceeding $3 \times 10^{-6} M_{\odot} \text{ yr}^{-1}$. So we expect no off-center burning of carbon during the accretion phase and that the C+O core grows until carbon ignites at the center.

Our numerical results are summarized in Figure 4. This figure shows the maximum WD mass $M_{\text{WD,max}}$ obtained in the binary evolution against the initial companion mass $M_{2,0}$ for various sets of parameters, $M_{\text{WD},0}$, $P_{\text{orb},0}$, and c_1 . Figure 4a shows examples for the parameter of $c_1 = 10$. We set a step of $0.5 M_{\odot}$ for the initial companion mass (except for a few models). The rightmost ends of these solid lines correspond to the model beyond which the mass transfer rate of $-\dot{M}_2$ quickly increases to 10^{-4} – $10^{-3} M_{\odot} \text{ yr}^{-1}$ and thus a common envelope is formed. We regard that two stars are merging into one. Solid lines are for the case that the companion fills its Roche lobe near ZAMS, i.e., $P_{\text{orb},0} \sim 0.5$ day. The WD mass reaches $M_{\text{WD,max}} \approx 2.7, 2.3, 1.9, 1.7,$ and $1.5 M_{\odot}$, for the initial WD mass of $M_{\text{WD},0} = 1.2, 1.1, 1.0, 0.9,$ and $0.8 M_{\odot}$, respectively. The dashed lines show the case that the companion fills its Roche lobe near the end of central hydrogen burning, i.e., $P_{\text{orb},0} \sim 1.5$ day. In this case, $M_{\text{WD,max}} \approx 2.3, 2.2, 2.0, 1.8,$ and $1.6 M_{\odot}$, for $M_{\text{WD},0} = 1.2, 1.1, 1.0, 0.9,$ and $0.8 M_{\odot}$, respectively. For the latter case (dashed lines) $M_{\text{WD,max}}$ smaller than that for the former case (solid lines) even for the same c_1 , $M_{\text{WD},0}$, and $M_{2,0}$. This is because the more evolved secondary has a larger mass transfer rate, $-\dot{M}_2$, and thus the duration of a high mass-accretion phase, in which period the WD grows quickly, is shorter than that of the near ZAMS case.

Figure 4b shows examples for the parameters of $c_1 = 3$ (solid lines) and $c_1 = 1$ (dotted lines), in which the companion

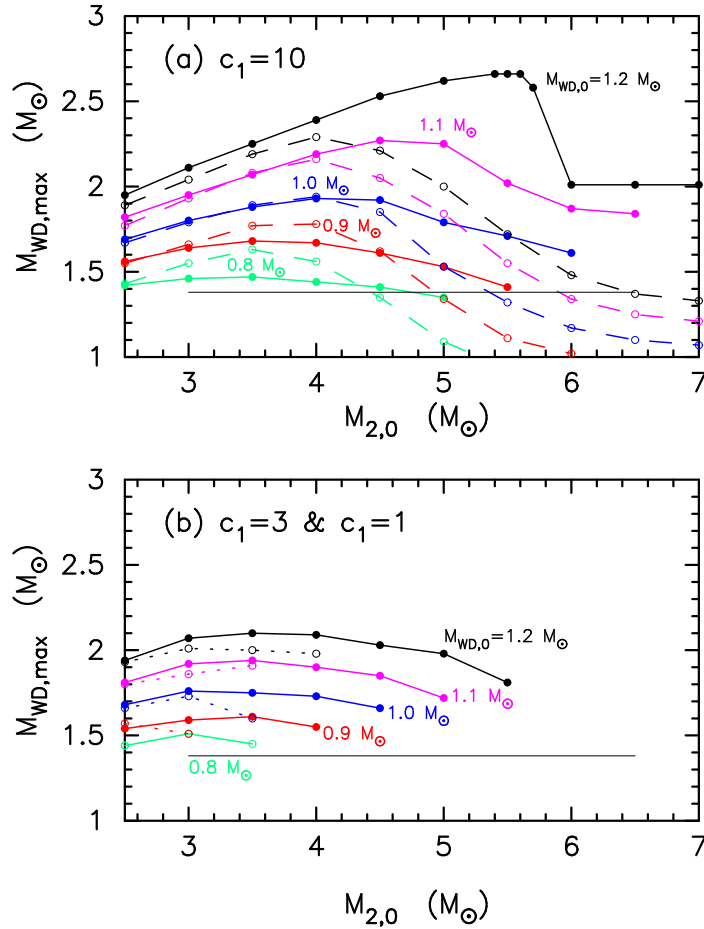


FIG. 4.— The maximum WD mass against the companion mass for the various initial WD masses and orbital periods. (a) $c_1 = 10$. The solid lines with small filled circle: the companion is slightly evolved off from ZAMS but still very close to ZAMS ($P_{\text{orb},0} \sim 0.5$ day) when the companion starts mass-transfer. The dashed lines with small open circle: the companion is close to the end of central hydrogen-burning ($P_{\text{orb},0} \sim 1.5$ day) when the companion starts mass-transfer. The horizontal thin solid line denotes $M_{\text{WD}} = 1.38 M_{\odot}$. (b) Same as those in (a) but for $c_1 = 3$ (solid lines) and $c_1 = 1$ (dashed lines), where the companion fills its Roche lobe near ZAMS, i.e., $P_{\text{orb},0} \sim 0.5$ day. See text for more details.

fills its Roche lobe near ZAMS, i.e., $P_{\text{orb},0} \sim 0.5$ day. The obtained maximum WD mass is smaller than that for $c_1 = 10$. In our previous work (Hachisu et al. 2008a), based on a simplified model of mass-transfer, we showed that more massive companions can avoid merging for larger c_1 -parameters. In the present work, we adopted a more realistic companion model which results in more accurate mass-transfer rates. Comparing Figure 4a with Figure 4b, we confirm that more massive companion avoids merging for a larger c_1 -parameter.

The maximum WD mass depends strongly on c_1 and $M_{\text{WD},0}$. To summarize, the maximum WD masses are $M_{\text{WD,max}} = 1.9, 1.9,$ and $2.3 M_{\odot}$ for $c_1 = 1, 3,$ and 10 , if the binary evolution starts from $M_{\text{WD},0} = 1.1 M_{\odot}$. If the binary evolution starts from a more massive initial WD mass of $M_{\text{WD},0} = 1.2 M_{\odot}$, a larger maximum WD mass is resulted as: $M_{\text{WD,max}} = 2.0, 2.1,$ and $2.7 M_{\odot}$ for $c_1 = 1, 3,$ and 10 , respectively.

3.2. Initial-final States of Binary Evolutions

We plot, in Figure 5, the initial parameter region that produces super-Chandrasekhar mass ($M_{\text{WD}} > 2.0 M_{\odot}$) SNe Ia in the $\log P - M_2$ (orbital period – secondary mass) diagram (hatched by magenta lines). Here we assume the metallicity of $Z = 0.02$ and the initial white dwarf mass of $M_{\text{WD},0} = 1.1 M_{\odot}$. A binary system initially inside the hatched region (above

$M_{\text{WD}} > 2.0 M_{\odot}$. The companion mass decreases with time, so that its position moves downward. When it reaches the hatched region (below), the mass-transfer rate drops below $\dot{M}_b = 3 \times 10^{-7} M_{\odot} \text{ yr}^{-1}$ and the Eddington-Sweet meridional circulation would redistribute angular momentum in the WD to trigger central carbon burning. Evolutionary paths of two typical cases of $M_{2,0} = 4.0 M_{\odot}$ companion star near ZAMS ($P_0 = 0.53$ day) and $M_{2,0} = 4.5 M_{\odot}$ companion near the end of central hydrogen burning ($P_0 = 1.48$ day) are followed by a thick magenta line with an arrow. Our calculated final states fall into a very narrow strip because all their evolutions stop at the same mass transfer rates of $\dot{M}_b = 3 \times 10^{-7} M_{\odot} \text{ yr}^{-1}$.

For comparison, we also added our previous results taken from Hachisu et al. (2008a,b, 1999a), where we assumed that a non-rotating C+O WD explodes at $M_{\text{WD}} = 1.38 M_{\odot}$ (Nomoto 1982a). The initial binary system inside the region encircled by a thin solid line (labeled “initial”) increases its WD mass up to the critical mass ($M_{\text{WD}} = 1.38 M_{\odot}$) and explodes in the regions encircled by a thick solid line (labeled “final”) for the white dwarf and main-sequence star (WD + MS) system (left) and the white dwarf and red giant (WD + RG) system (right). We have found no super-Chandrasekhar mass SN Ia ($M_{\text{WD}} > 2.0 M_{\odot}$) region for the WD+RG systems mainly because mass of the companion is too small to supply much matter to the WD. Currently known positions

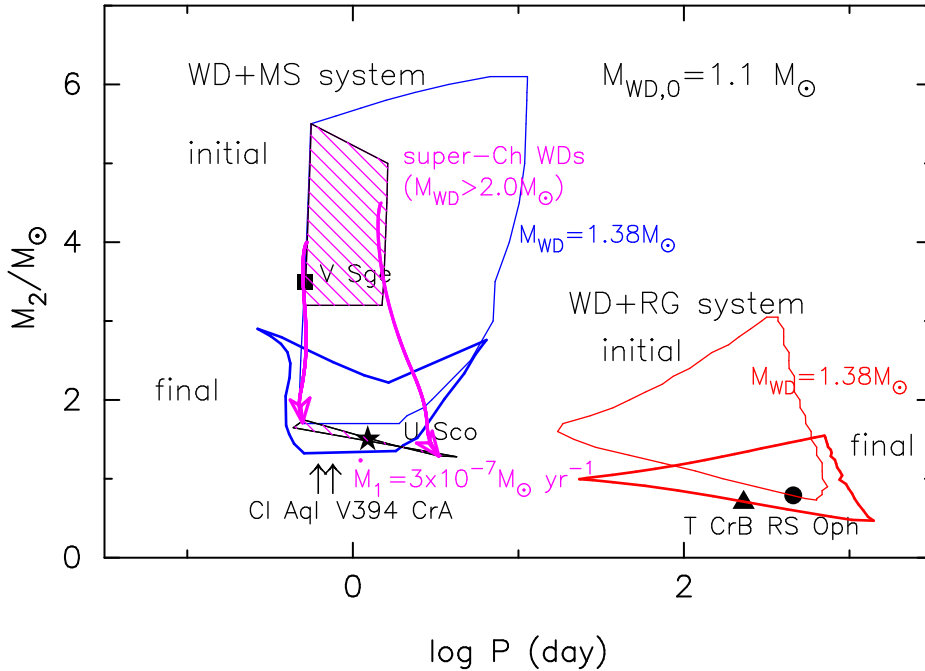


FIG. 5.— The regions that produce super-Chandrasekhar mass ($M_{\text{WD}} > 2.0 M_{\odot}$) SNe Ia are plotted in the $\log P - M_2$ (orbital period – secondary mass) plane (hatched by magenta lines). Here we assume the metallicity of $Z = 0.02$ and the initial WD mass of $M_{\text{WD},0} = 1.1 M_{\odot}$. The initial system inside the hatched region (above) increases its WD mass up to a super-Chandrasekhar mass of $M_{\text{WD}} > 2.0 M_{\odot}$ and then reaches the hatched region (below) where the mass-transfer rate drops below $\dot{M}_b = 3 \times 10^{-7} M_{\odot} \text{ yr}^{-1}$. Evolutionary paths of two typical cases ($4.0 M_{\odot}$ companion star near ZAMS and $4.5 M_{\odot}$ companion near the end of central hydrogen burning) are traced by a thick magenta line with an open arrow. We also added the previous results taken from Hachisu et al. (2008a,b, 1999a), where we assumed that a non-rotating C+O WD explodes at $M_{\text{WD}} = 1.38 M_{\odot}$. The initial system inside the region encircled by a thin solid line (labeled “initial”) increases its WD mass up to the critical mass ($M_{\text{WD}} = 1.38 M_{\odot}$) and explodes in the regions encircled by a thick solid line (labeled “final”) for the white dwarf and main-sequence star (WD + MS) system (left) and the white dwarf and red giant (WD + RG) system (right). Currently known positions of Galactic recurrent novae and supersoft X-ray sources are indicated by a star mark (*) for U Sco (e.g., Hachisu et al. 2000a), a triangle for T CrB (Belczyński & Mikolajewska 1998), a filled circle for RS Oph (Brandi et al. 2009), a square for V Sge (Hachisu & Kato 2003b). Arrows indicate V394 CrA and CI Aql, because their companion masses are not known.

of some Galactic recurrent novae and supersoft X-ray sources are indicated by a star mark (*) for U Sco (e.g., Hachisu et al. 2000a), a triangle for T CrB (Belczyński & Mikolajewska 1998), a filled circle for RS Oph (Brandi et al. 2009), a square for V Sge (Hachisu & Kato 2003b), and by arrows for the two recurrent novae, V394 CrA and CI Aql, because mass of a companion is not yet accurately obtained. Two subclasses of the recurrent novae, the U Sco type and the RS Oph type, correspond to the WD + MS channel and the WD + RG channel of SNe Ia, respectively.

Hachisu & Kato (2001) summarized the mass transfer rates of Galactic recurrent novae in their Table 2, in which only U Sco has a large mass transfer rate enough to support differential rotation, i.e., the mass transfer rate is $\sim 2.5 \times 10^{-7} M_{\odot} \text{ yr}^{-1}$ and the net growth rate of C+O core is $\sim 1.0 \times 10^{-7} M_{\odot} \text{ yr}^{-1}$. Therefore, U Sco may have a super-Chandrasekhar mass WD. Thoroughgood et al. (2001) observationally estimated the WD mass of U Sco to be $M_{\text{WD}} = 1.55 \pm 0.24 M_{\odot}$ in the 1999 outburst. The systematic error is, however, too large to draw a definite conclusion for super-Chandrasekhar mass, so we strongly encourage more accurate observations to determine the WD mass in U Sco.

3.3. Stability of Mass-accreting, Differentially Rotating WDs

In the present paper, we simply assume that the mass-accreting, differentially rotating WDs are stable and can accrete mass from the companion as long as its mass accretion rate is larger than $\dot{M}_b = 3 \times 10^{-7} M_{\odot} \text{ yr}^{-1}$. This assumption is based on the results in Yoon & Langer (2004). However, they did not incorporate the possibility of baroclinic instability in

the WD mainly because equi-density and equi-pressure lines are essentially parallel in the WD due to high degeneracy. If the baroclinic instability could occur (Fujimoto 1993), angular momentum is effectively transported in a shorter timescale than the accretion timescale, so that a rigid rotation is realized (Saio & Nomoto 2004). If this is the case, suggested super-Chandrasekhar mass WDs would not be realized in the SD scenario.

Recently, Piro (2008) concluded, based on Fujimoto’s (1993) baroclinic instability criterion, that baroclinic instabilities bring the WD very close to solid-body rotation during accretion phase, which makes it difficult to grow a WD mass substantially past the Chandrasekhar mass. However, we should notice that Fujimoto’s criterion on baroclinic instability is just a necessary condition but not a sufficient condition. In this sense, Piro’s (2008) result is not always correct. We must keep in mind that he showed only a possibility for baroclinic instability on mass-accreting WDs but not an occurrence of baroclinic instability. On the other hand, the Richardson criterion on the Kelvin-Helmholtz instability is also a necessary condition but has ever been tested for a variety of basic (plane-parallel) flows as a sufficient condition for the instability (see, e.g., Fujimoto 1993). Yoon & Langer’s (2005) stability criterion was based on the Richardson criterion of the Kelvin-Helmholtz instability. Therefore, we expect that the true mixing instability for redistribution of angular momentum occurs somewhere between the Richardson criterion and Fujimoto’s (1993) criterion.

If we assume Yoon & Langer’s (2005) stability criterion (the Richardson criterion) and extrapolate their formula on

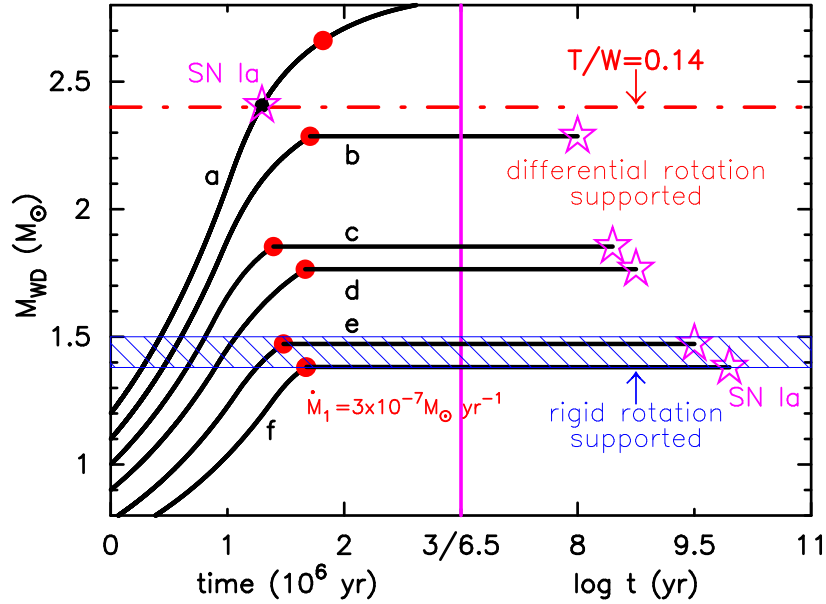


FIG. 6.— Schematic illustration for evolutions of the WD mass against time. Time starts when the secondary fills its Roche lobe and it is switched from linear to logarithmic at $t \approx 3 \times 10^6$ yr (a vertical magenta line). The evolutionary lines in the left (part) to the magenta line are taken from our numerical results while those in the right (part) are just schematic illustrations. From top to bottom: (a) $M_{\text{WD},0} = 1.2 M_{\odot}$, $M_{2,0} = 5.5 M_{\odot}$, $P_0 = 0.57$ day, $c_1 = 10$. Same model as the model in Figure 2b. In this model, $T/|W|$ exceeds 0.14 before the mass accretion rate becomes lower than $\dot{M}_b = 3 \times 10^{-7} M_{\odot} \text{ yr}^{-1}$. We expect an SN Ia explosion at the position of magenta star mark ($M_{\text{WD}} \approx 2.4 M_{\odot}$) soon after a secular instability sets in. (b) $M_{\text{WD},0} = 1.1 M_{\odot}$, $M_{2,0} = 4.7 M_{\odot}$, $P_0 = 0.54$ day, $c_1 = 10$. Same model as the model in Figure 2a, where $T/|W|$ does not exceed 0.14 before $\dot{M}_1 < \dot{M}_b = 3 \times 10^{-7} M_{\odot} \text{ yr}^{-1}$. Loss or redistribution of angular momentum leads to an increase in the central density until carbon is ignited to induce SN Ia explosion ($M_{\text{WD}} \approx 2.3 M_{\odot}$). The delay time depends on the timescales of angular momentum loss or redistribution. It may take a time of order 10^8 – 10^9 yr if angular momentum redistribution occurs due to Eddington-Sweet circulation (Yoon & Langer 2004). (c) $M_{\text{WD},0} = 1.0 M_{\odot}$, $M_{2,0} = 4.5 M_{\odot}$, $P_0 = 1.46$ day, $c_1 = 10$. The WD mass reaches $M_{\text{WD}} = 1.85 M_{\odot}$, which is differential-rotation-supported. (d) $M_{\text{WD},0} = 0.9 M_{\odot}$, $M_{2,0} = 3.5 M_{\odot}$, $P_0 = 1.38$ day, $c_1 = 10$. The WD mass reaches $M_{\text{WD}} = 1.76 M_{\odot}$, which is differential-rotation-supported. (e) $M_{\text{WD},0} = 0.8 M_{\odot}$, $M_{2,0} = 4.9 M_{\odot}$, $P_0 = 0.52$ day, $c_1 = 10$. The WD mass reaches $M_{\text{WD}} = 1.47 M_{\odot}$, which can be supported by rigid rotation (Hachisu 1986; Uenishi et al. 2003). Therefore, it may take a longer time than the case of differentially-rotating-supported WDs. (f) $M_{\text{WD},0} = 0.7 M_{\odot}$, $M_{2,0} = 3.0 M_{\odot}$, $P_0 = 0.47$ day, $c_1 = 5$. The WD mass reaches $M_{\text{WD}} = 1.38 M_{\odot}$, which can also be supported by rigid rotation.

$T/|W|$ (their Equation [29]) to higher masses, where T and W are the rotational and gravitational energies of the WD, respectively, angular momentum redistribution could occur when $T/|W|$ exceeds 0.14 and a secular instability sets in. This instability occurs at $M_{\text{WD}} \approx 2.4 M_{\odot}$ (see also Hachisu 1986). At this time, the WD would be too massive to keep hydrostatic equilibrium and contracts on a much shorter timescale due to angular momentum transport. As a result of such a rapid compression, the WD eventually ignites explosive carbon burning in the central region to give rise to an SN Ia explosion. If super-Chandrasekhar mass SNe Ia occur in this way, the WD mass can be as massive as up to $2.4 M_{\odot}$. To confirm this prediction, accurate estimates of the ejecta masses, in which asphericity is taken into account, would be important.

3.4. Evolutions in Three Mass Ranges of Exploding WDs

If we apply the above discussion to the super-Chandrasekhar mass WDs, we may further discuss the fate of the WDs. There are three characteristic mass ranges of exploding WDs depending on the secular instability and rotation law: (1) $M_{\text{WD}} > 2.4 M_{\odot}$ (a secular instability at $T/|W| = 0.14$), (2) $M_{\text{WD}} = 1.5$ – $2.4 M_{\odot}$ (differential rotation), and (3) $M_{\text{WD}} = 1.38$ – $1.5 M_{\odot}$ (rigid rotation).

3.4.1. SNe Ia triggered by Secular Instability: SN 2007if/SN 2009dc-like

For very massive WDs, a secular instability sets in at $T/|W| = 0.14$ and the WD explodes as an SN Ia when it reaches $2.4 M_{\odot}$. For example, the model of $M_{\text{WD},0} = 1.2 M_{\odot}$,

$M_{2,0} = 5.5 M_{\odot}$, $P_0 = 0.57$ day, and $c_1 = 10$ (Figure 2b) reaches $T/|W| = 0.14$ at $t = 1.28 \times 10^6$ yr. This evolution model is also shown in Figure 6 by the uppermost line (“a” is attached to the line). Therefore, we expect an SN Ia explosion to occur at the magenta star mark because the timescale of the secular instability is much shorter than the mass-accreting timescale. This kind of binary evolution corresponds to the very luminous super-Chandrasekhar mass SNe Ia such as SN 2007if and SN 2009dc. It is interesting that these brightest super-Chandrasekhar mass SNe Ia are the youngest among our models (younger than a few hundred Myr).

3.4.2. SNe Ia triggered by Loss or Redistribution of Angular Momentum: SN 2003fg/SN 2006gz-like

For $M_{\text{WD}} = 1.5$ – $2.4 M_{\odot}$, $T/|W|$ does not exceed 0.14. For example, the model for the initial parameters of $M_{\text{WD},0} = 1.1 M_{\odot}$, $M_{2,0} = 4.7 M_{\odot}$, $P_0 = 0.54$ day, and $c_1 = 10$ (Figure 2a) reaches $M_{\text{WD}} = 2.3 M_{\odot}$ before the accretion rate drops to $\dot{M}_1 < \dot{M}_b = 3 \times 10^{-7} M_{\odot} \text{ yr}^{-1}$ at the red filled circle in Figure 6 (line b). We also show two other examples. One is for the initial parameters of $M_{\text{WD},0} = 1.0 M_{\odot}$, $M_{2,0} = 4.5 M_{\odot}$, $P_0 = 1.46$ day, and $c_1 = 10$. In this case, the WD mass reaches $M_{\text{WD}} = 1.85 M_{\odot}$, which is also differential-rotation-supported (line c in Figure 6). The other is for $M_{\text{WD},0} = 0.9 M_{\odot}$, $M_{2,0} = 3.5 M_{\odot}$, $P_0 = 1.38$ day, and $c_1 = 10$. The WD mass reaches $M_{\text{WD}} = 1.76 M_{\odot}$, which is again differential-rotation-supported (line d in Figure 6).

However, the WD does not explode soon after the WD mass has reached the maximum mass (1.5 – $2.3 M_{\odot}$), because the central density is low so that central carbon is not ignited yet.

After some time, loss or redistribution of angular momentum would lead to an increase in the central density of the WD. As a result, carbon is ignited to induce an SN Ia. This waiting time depends entirely on the timescale of angular momentum loss or redistribution. It is an order of 10^8 – 10^9 yr if angular momentum redistribution occurs due to the Eddington-Sweet circulation (Yoon & Langer 2004). If direct loss of angular momentum occurs in a much shorter timescale (due to magneto-dipole radiation or so), it could be much shorter than $\sim 10^8$ yr. In any case, it is shorter than 10^8 – 10^9 yr. Therefore we suggest that these relatively young SNe Ia correspond to the “prompt” component. We regard that this kind of binary evolution corresponds to super-Chandrasekhar mass SNe Ia such as SN 2003fg/SN 2006gz, not so extremely luminous as SN 2007if/SN 2009dc.

3.4.3. SNe Ia triggered by Loss of Angular Momentum: normal SNe Ia

For $M_{\text{WD}} < 1.5 M_{\odot}$, WDs could be rigidly rotating. For example, line e in Figure 6 shows the case of $M_{\text{WD},0} = 0.8 M_{\odot}$, $M_{2,0} = 4.9 M_{\odot}$, $P_0 = 0.52$ day, and $c_1 = 10$. The WD mass reaches $M_{\text{WD}} = 1.47 M_{\odot}$, which can be supported by rigid rotation (e.g., Hachisu 1986; Uenishi et al. 2003). Also, line f in Figure 6 depicts the case of initial parameters of $M_{\text{WD},0} = 0.7 M_{\odot}$, $M_{2,0} = 3.0 M_{\odot}$, $P_0 = 0.47$ day, and $c_1 = 5$. The WD mass reaches $M_{\text{WD}} = 1.38 M_{\odot}$ at the red filled circle. The WD can also be supported by rigid rotation.

The WD will eventually explode as an SN Ia after the WD spins down and the central density increases high enough to ignite carbon. This spinning-down timescale depends highly on the subtraction mechanism of angular momentum from the WD such as magneto-dipole radiation in a strongly magnetized WD. Recently, Ilkov & Soker (2011) reexamined the timescale of spin-down due to r-mode gravitational radiation and showed that r-mode instability is not significant in spinning down WDs (see also Lindblom 1999; Yoon & Langer 2005). Instead, they suggested that magneto-dipole radiation leads to spinning-down in a typical timescale of $< 10^9$ yr in WDs as massive as $M_{\text{WD}} \gtrsim 1.6 M_{\odot}$ but in a typical timescale of $> 10^9$ yr in $M_{\text{WD}} = 1.4$ – $1.5 M_{\odot}$. If it is the case, these rigidly-rotating WDs of $M_{\text{WD}} = 1.38$ – $1.5 M_{\odot}$ may correspond to the “tardy” component, suggesting that the companion has evolved off to a white dwarf when the WD explodes as an SN Ia (Justham 2011; Di Stefano et al. 2011).

There is an example of WDs that had once been extremely spun-up but now are very slowly spinning down. Recently a massive, fast spinning WD with a spin period of $P_{\text{spin}} = 13.2$ s and a mass of $M_{\text{WD}} = 1.28 \pm 0.05 M_{\odot}$ was found in a binary system HD 49798/RX J0648.0–4418 ($P_{\text{orb}} = 1.55$ day), which is consisting of a hot subdwarf and a WD (e.g., Merghetti et al. 2011). This spin period is only a factor of two longer than the critical spin period². The spin-down rate is too small to be detected, i.e., $\dot{P}_{\text{spin}} < 9 \times 10^{-13}$ s s⁻¹. Merghetti et al. (2011) estimated a very weak magnetic field of $B < 1$ kG at the WD surface. In such a low magnetic field, the spin-down rate due to magneto-dipole radiation should be so small that we expect a very long decay time

² The total angular momentum and rotational energy are $J = 0.749 \times 10^{50}$ erg s and $T = 0.315 \times 10^{50}$ erg, respectively, at the critical rotation from Table 4 of Hachisu (1986). Then we have $\Omega_{\text{cr}} = 2T/J = 0.841$ rad s⁻¹, so the critical spin period is $P_{\text{spin,cr}} = 2\pi/\Omega_{\text{cr}} = 7.47$ s for a rigidly rotating $1.28 M_{\odot}$ WD.

($> 10^9$ yr) of the rapidly rotating WD (see, e.g., Equation 10 of Ilkov & Soker 2011).

4. POSSIBLE EVOLUTIONARY PATHS TO MASSIVE C+O WD BINARIES

In the previous section, we present candidate binaries that have an evolutionary path toward a super-Chandrasekhar mass progenitor. Such binaries should consist of a very massive C+O WD ($M_{\text{WD},0} \sim 1.1$ – $1.2 M_{\odot}$) and an intermediate-mass ($M_{2,0} \sim 4$ – $5 M_{\odot}$) companion star with an orbital period of $P_{\text{orb},0} \sim 0.5$ – 1.5 days. These massive C+O WDs, however, have not been expected mainly because dust-driven wind mass-loss prevents the C+O WDs from growing in their mass in the AGB phase (e.g., Herwig 2005, for a recent review of AGB stars). For example, Umeda et al. (1999) calculated evolutions of 3–9 M_{\odot} stars for the metallicity of $Z = 0.001$ – 0.03 from ZAMS until the second dredge-up stage, that is, until the early AGB phase. They showed that an upper limit of C+O core mass is $M_{\text{C+O}} = 1.07 M_{\odot}$ for the initial MS mass of $M_i = 8.1 M_{\odot}$ ($Z = 0.02$) and for $M_i = 7.1 M_{\odot}$ ($Z = 0.004$). If this $1.07 M_{\odot}$ upper limit is applied to all the C+O WDs, both the SD and DD scenarios hardly explain super-luminous SNe Ia such as SN 2007if/SN 2009dc. In this section, we discuss possible evolutionary paths toward our candidates.

4.1. Metallicity Effects of C+O Core Masses

In close binaries, the primary star fills its Roche lobe before it evolves to an AGB star. In relatively wide binaries, a star will evolve further beyond the early AGB phase (the second dredge-up stage). In the AGB phase, hydrogen shell-burning produces helium and that helium piles up on the C+O core. The helium intermittently ignites to trigger a shell-flash, making a thermal pulse phase (TP-AGB phase). The C+O core mass would increase further beyond $1.07 M_{\odot}$ during the TP-AGB phase until all hydrogen envelope is lost by winds (or stripped away by the companion star). How much mass can be added to the C+O core during the TP-AGB phase? We roughly assume an average increasing rate of the core mass from hydrogen shell-burning rate, $\dot{M}_c \sim 5 \times 10^{-7} M_{\odot} \text{ yr}^{-1}$, during the TP-AGB phase (see Equation [1]). On the other hand, the dust-driven wind mass-loss rates are observationally estimated to be about $\dot{M}_w \sim 3 \times 10^{-5} M_{\odot} \text{ yr}^{-1}$ (de Beck et al. 2010), where the mass-loss rate levels off for stars with longer pulsation periods of $\gtrsim 850$ days. Therefore, the ratio of the wind mass-loss rate to the mass-accretion rate is about $\zeta \equiv \dot{M}_w/\dot{M}_c \sim 60$. This simply suggests that the upper limit for the increase in the core mass is about $\Delta M_c \approx (M_{1,i} - M_{1,c})/\zeta \sim 6 M_{\odot}/60 \sim 0.1 M_{\odot}$, where $M_{1,i}$ and $M_{1,c}$ are the initial mass and the C+O core mass of the primary, respectively. Furthermore, recent models of massive AGB stars show very efficient third dredge-up and hot-bottom burning (e.g., Herwig 2005, for a recent review), both of which reduce the core growth. Therefore the core of massive AGB stars seems to hardly grow (see, e.g., Weidemann 2000, for initial-final mass relation of single stars).

Many authors have calculated the evolutions of TP-AGB stars, but full calculation through thermal pulses is extremely time-consuming. Thus the evolution has been often followed only through a small number of pulses and then replaced by synthetic models towards the end of the AGB. Very recently, a few full AGB calculations appeared including a number of thermal pulses until the end of the AGB phase (e.g., Karakas 2010; Siess 2010; Ventura & D’Antona 2009;

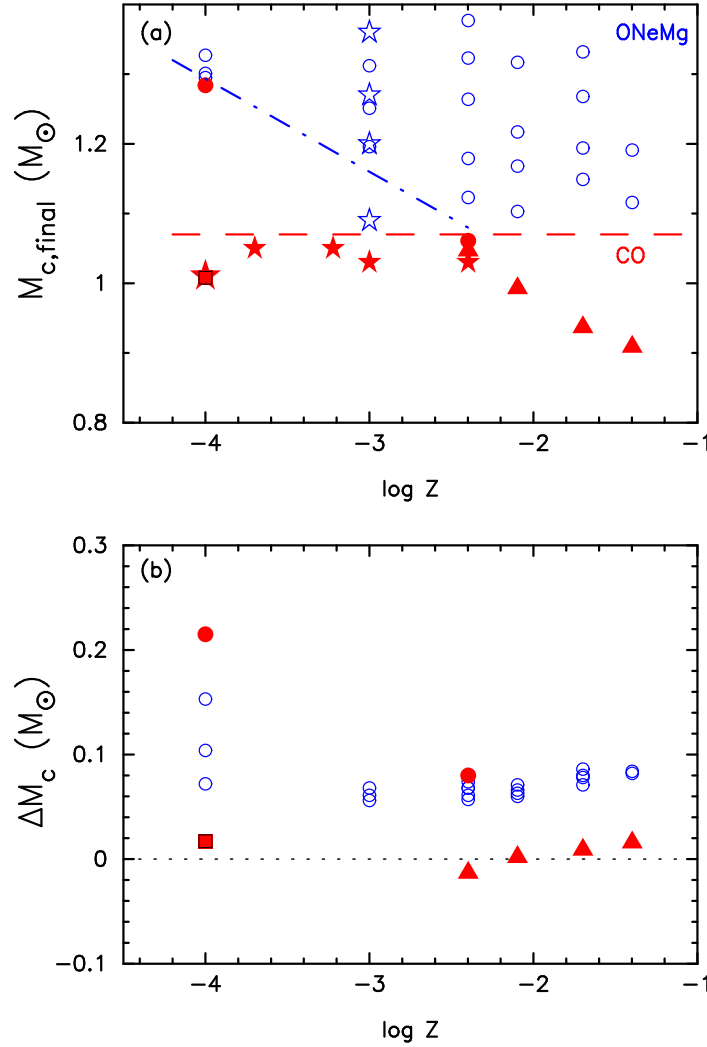


FIG. 7.— (a) Final core masses of AGB stars against metallicity (Z). Here $M_{c,\text{final}}$ is the final core mass of AGB evolutions in solar mass units. Different symbols denote different authors' results. Red symbols indicate C+O cores while blue O+Ne+Mg cores. Circles: C+O/O+Ne+Mg cores taken from Siess (2010). Triangles: C+O cores taken from Weiss & Ferguson (2009). Stars: C+O/O+Ne+Mg cores taken from Ventura & D'Antona (2009) and Ventura & D'Antona (2011). Squares: C+O cores taken from Karakas (2010). The red dashed line indicates $1.07 M_{\odot}$ of C+O cores. The blue dash-dotted line denotes a line below which C+O cores may exist for lower metallicities of $Z \leq 0.002$ estimated from the results of Siess (2010). (b) Core-mass increase, ΔM_c , after the first thermal pulse until the end of AGB evolution against metallicity. Symbols are the same as those in (a).

Weiss & Ferguson 2009). The resultant WD mass, however, depends strongly on the adopted mass-loss law, extra mixing (overshooting of convection), hot bottom burning, etc. Different laws gave different results.

Figure 7 shows such diverse of resulting WD masses through full TP-AGB calculations. All red filled symbols indicate the C+O core masses after the AGB evolution for the initial ZAMS mass of $M_i \geq 6 M_{\odot}$. On the other hand, blue open symbols denote the O+Ne+Mg core masses at the end of the AGB evolution for the initial ZAMS mass of $M_i \geq 6.5 M_{\odot}$. Different symbols correspond to different authors: circles (Siess 2010), squares (Karakas 2010), triangles (Weiss & Ferguson 2009), and stars (Ventura & D'Antona 2009, 2011).

Ventura & D'Antona's (2009, 2011) results show $\sim 1.07 M_{\odot}$ as an upper limit of C+O WDs for a wide range of metallicities, i.e., for $Z = 0.0001\text{--}0.004$. On the other hand, Siess's (2010) results show a considerable increase in the C+O core mass for very low metallicities such as $Z \lesssim 0.002$. The main differences probably come from the different treatments of wind mass-loss during the TP-AGB and possibly

extra-mixing, because Siess (2010) assumed Schwarzschild criterion of convection, which prevents the third dredge-up, and also assumed Vassiliadis & Wood's (1993) mass-loss rate, which makes the duration of the TP-AGB phase much longer than that of Blöcker's (1995) formalism adopted by Ventura & D'Antona (2009). Ventura & D'Antona (2011) showed that Vassiliadis & Wood's formalism gives about 9 times more thermal pulses than Blöcker's formulation for the same initial mass of $7 M_{\odot}$ ($Z = 0.001$), i.e., 348 vs. 38, because of weaker wind mass-loss rates and thus a longer duration of the TP-AGB phase. If Vassiliadis & Wood's one is the case, we have C+O WDs more massive than $1.1 M_{\odot}$ for lower metallicities, which can open an evolutionary route to super-Chandrasekhar mass SNe Ia as massive as $2.3\text{--}2.7 M_{\odot}$.

These two formalisms by Vassiliadis & Wood (1993) and Blöcker (1995) do not explicitly include metallicity effects. Observationally there are some suggestions on metallicity effects of AGB winds. Local galaxies with low Z show some evidence for a deficiency in the number of planetary nebulae (PNe) at $[\text{Fe}/\text{H}] \lesssim -1$ (Magrini et al. 2003; Zijlstra 2004). The deficiency of PNe suggests that the mass-loss rates are not

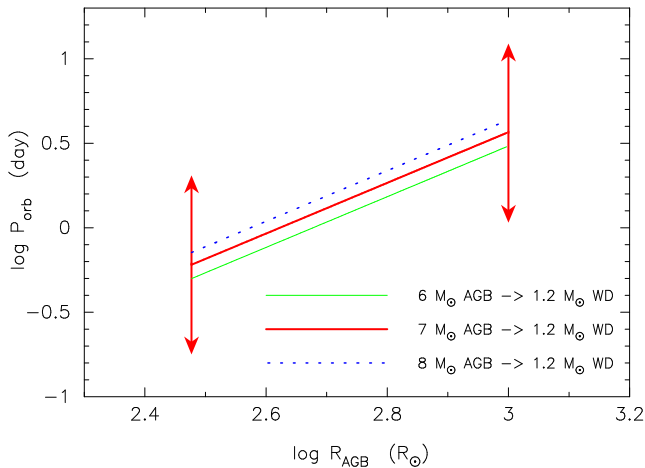


FIG. 8.— Final orbital periods against the radii of AGB stars just before the common envelope evolution. We assume that the AGB star fills its Roche lobe when the C+O core grows to $1.2 M_{\odot}$ and a common envelope evolution starts. We plot three cases of mass of the AGB star, i.e., 6 (green thin), 7 (red thick), and $8 M_{\odot}$ (blue dotted). Vertical arrows indicate upper/lower dispersions of the factor $\alpha\lambda$ in Equation (4). (See Equations [5] and [6]).

as high as those observed in metallicities of $[\text{Fe}/\text{H}] \gtrsim -1$. In other words, a superwind does not blow in lower metallicity environment (Zijlstra 2004). These changes of behavior occur at $[\text{Fe}/\text{H}] \approx -1$ (see also Bowen & Willson 1991, for a theoretical discussion on this metallicity effect), suggesting that, in lower Z ($[\text{Fe}/\text{H}] \lesssim -1$) environments, C+O WDs possibly become more massive than those in higher Z ($[\text{Fe}/\text{H}] \gtrsim -1$) environments.

From these circumstances, we expect that AGB stars produce C+O WDs with mass higher than $1.1 M_{\odot}$ in lower metallicities of $Z \lesssim 0.002$. Since the mass loss is relatively weak in lower metallicity AGB stars, the C+O core is likely to grow as massive as $1.2 M_{\odot}$ or more before the binary undergoes a common envelope evolution. In such a case, the maximum C+O WD mass can reach $2.3\text{--}2.7 M_{\odot}$ by accretion (see Figure 4a). Observational suggestions on massive C+O WDs and low metallicity environments of super- M_{Ch} SNe Ia will be discussed in Section 5.3.

Finally, we comment on Nomoto & Kondo’s (1991) upper limit for the initial C+O WD mass: $M_{\text{WD},0} \lesssim 1.2 M_{\odot}$ for SN Ia explosions (see Figure 4 of Nomoto & Kondo 1991). This upper limit, however, does not apply to our super-Chandrasekhar mass WDs. This upper limit is valid only when the central part of the WD stays cold so that central carbon burning leads to a collapse instead of explosion. In the normal case of Chandrasekhar mass SNe Ia, compressional heat due to mass-accretion does not reach the central part in a short timescale, e.g., that a WD grows from 1.3 to $1.38 M_{\odot}$. On the other hand, for super-Chandrasekhar mass WDs, the timescale of mass-accretion becomes much (a few to several times) longer because it takes more than a few to several times for a WD to grow, e.g., from 1.3 to $1.8 M_{\odot}$. At the time of central carbon ignition, the central part has been heated up, thus central carbon burning leads to an SN Ia explosion.

4.2. First Common Envelope Evolution and Binary Orbital Period

Now we examine the condition for the initial orbital period ($P_{\text{orb},0} = 0.5\text{--}1.5$ days) to be realized when an AGB star with a core mass of $M_{\text{C+O}} = 1.1\text{--}1.2 M_{\odot}$ undergoes a common envelope evolution. de Marco et al. (2011) analyzed the post

common envelope evolution systems with the relation of

$$-G \frac{M_c(M_e/2 + M_c)}{\lambda R} = -\alpha G \left[\frac{M_c M_2}{2a_f} - \frac{(M_c + M_e) M_2}{2a_i} \right], \quad (4)$$

where M_c and M_e are the giant primary’s core mass and the primary’s envelope mass, a_f and a_i the final and initial separation of the binary, M_2 the secondary’s mass, which is not changed during the common envelope evolution, λ is the number of order unity which depends on the mass distribution of the primary’s envelope (λR is effectively the mass-weighted mean radius of the envelope), and α the efficiency parameter of order unity. They obtained λ and α for AGB stars as

$$\lambda_{\text{AGB}} = (0.237 \pm 0.021) + (0.032 \pm 0.006) \times \frac{M_{\text{MS}}}{M_{\odot}}, \quad (5)$$

$$\log \alpha = (-1.4 \pm 0.2) - (1.2 \pm 0.2) \log \frac{M_2}{M_1}, \quad (6)$$

where M_{MS} is the main-sequence mass of the AGB star, and M_1 and M_2 are the primary and secondary masses just before the common envelope evolution, respectively. We do not know the exact radius of TP-AGB stars just before the common envelope evolution, so we roughly assume the radius of $R \sim 300\text{--}1000 R_{\odot}$ (see, e.g., Figures 1 and 2 of Webbink 2007), and the C+O core mass of $1.2 M_{\odot}$, and $M_1 = 6, 7,$ and $8 M_{\odot}$, and $M_2 = 4 M_{\odot}$. Then we have $a_i \sim 700\text{--}2200 R_{\odot}$. Substituting these values into Equations (4), (5), and (6), we estimate the final separation of the binary. Figure 8 shows the orbital period of the binary against the radius of the AGB star just before the common envelope evolution. We obtain rather short separations and orbital periods of $a_f \sim 5\text{--}17 R_{\odot}$ and $P_{\text{orb},0} \sim 0.6\text{--}3.6$ days for $M_{1,i} = 7 M_{\odot}$, $M_{1,\text{C+O}} = M_{\text{WD},0} = 1.2 M_{\odot}$, and $M_{2,i} = 4 M_{\odot}$. Incorporating ambiguity of Equations (4)–(6) in common envelope evolution, the resultant binary periods lie possibly in the region of $0.5\text{--}1.5$ days, which is consistent with our requirement for super-Chandrasekhar mass SNe Ia of $M_{\text{WD}} \sim 2.3\text{--}2.7 M_{\odot}$.

5. DISCUSSION

5.1. Comparison with Other SD Models

Chen & Li (2009) calculated binary evolutions to SNe Ia without including mass-stripping effect. Our results can be compared with their cases of very short WD wind phases because of small mass-stripping effects. Chen & Li (2009) obtained the maximum WD mass of $1.75 M_{\odot}$ at $t \sim 1.5$ Myr (after the companion fills its Roche lobe) for $M_{\text{WD},0} = 1.2 M_{\odot}$, $M_{2,0} = 2.5 M_{\odot}$, and $P_{\text{orb},0} = 1$ day (with $c_1 = 0$ in our definition). We obtained $M_{\text{WD}} = 1.87, 1.88, 1.89 M_{\odot}$ at $t \sim 1.5$ Myr for the same initial model with $c_1 = 1, 3,$ and 10 , respectively. Our results are consistent with theirs. The small difference of $\sim 0.1 M_{\odot}$ might stem from the difference in the mass-accretion rates onto the WD; Chen & Li assumed smaller accretion rates than ours by taking into account centrifugal force, thus they get a smaller WD mass.

5.2. Detectability of SD signatures

In a recent review, Howell (2011) listed four major arguments strongly against the existing SD scenarios: (1) very few supersoft X-ray sources have been found in galaxies; (2) no shock interaction between ejecta and a companion star has been seen; (3) no hydrogen lines have been detected; (4) no explanation of super-Chandrasekhar mass type Ia supernovae has been given.

As for the first argument, although being not directly related to the super-Chandrasekhar mass models, Gilfanov & Bogdán (2010) claimed that observed soft X-ray fluxes of early type galaxies contradict the SD scenario based on simple assumptions. However, Hachisu et al. (2010) showed that realistic evolutionary models of the SD systems spend a large fraction of the life time in the optically thick wind phase and the recurrent nova phase rather than the supersoft X-ray source (SSS) phase. Thus the SSS phase lasts only for a few hundred thousand years. This is by a factor of ~ 10 shorter than those adopted by Gilfanov & Bogdán (2010) where the SN Ia progenitor WD was assumed to spend most of its life as a SSS. The X-ray luminosity of the SSS has a large uncertainty because of the uncertain atmospheric model of mass-accreting WDs and absorption of soft X-rays by the companion star's cool wind material. Thus adopting an average of the observed fluxes of existing symbiotic SSSs, Hachisu et al. (2010) showed that the observed X-ray fluxes in early type galaxies obtained by Gilfanov & Bogdán (2010) are rather consistent with the SD scenario.

As for the second (and third) points, Howell (2011) claimed that there should be some observational evidence of shock interaction between ejecta and the companion star (Kasen 2010) such as distortions in early-time light curves of SNe Ia, especially for a RG companion, but no such signatures have been observed. This is problematic for the SD scenario of WD+RG systems (Hayden et al. 2010; Bianco et al. 2011, see, however, a different (rather contradict) result by Ganeshalingam et al. (2011)). These shocking signatures predicted in Kasen (2010) are based on the assumption that the companion fills its Roche lobe. However, if the binary separation, a , is much larger than the companion radius, R , i.e., $a \gg R$, the solid angle subtended by the companion would be much smaller, and so would be the effect of shocking. Justham (2011) and Di Stefano et al. (2011) argued that the donor star in the SD scenario might shrink rapidly before the WD explosion, because it would exhaust its hydrogen-rich envelope during a long spinning down time of the rapidly rotating WD until the SN Ia explosion. In such a case, the companion star would be much smaller than its Roche lobe, reducing the shocking signature, which also explains the lack of hydrogen in the spectra of SNe Ia.

In our super-Chandrasekhar mass SN Ia models, the SN Ia explosion occurs after the mass of the main-sequence (MS) secondary decreases to as small as $1.5\text{--}1.8 M_{\odot}$ (see, e.g., two evolution models in Figure 5). Impact with such a low mass MS companion would not produce a large distortion in early-time SN Ia light curves (see, e.g., Figure 3 of Kasen 2010), so no detection of distortion is not a problem at least for our super-Chandrasekhar mass models.

As for the third disfavor point, Howell (2011) claimed that if WDs grow to become SNe Ia via hydrogen accretion, there should be some indication of hydrogen in some form, but no such indication has been found, e.g., in radio emission (Panagia et al. 2006) nor in stripped ejecta from the companion (Marietta et al. 2000). Justham (2011) and Di Stefano et al. (2011) argued that the donor star in the SD scenario would shrink rapidly to become a helium white dwarf before the WD explosion, having exhausted its hydrogen-rich envelope. Therefore, no detection of hydrogen would naturally be expected.

In our super-Chandrasekhar mass SN Ia models, the SN Ia explosion occurs after the mass of the main-sequence (MS) secondary decreases to as small as $\sim 2.0 M_{\odot}$ (see, e.g., model

a in Figure 6). Impact with such a low mass MS companion would lead to a strip of hydrogen-rich matter as massive as $\sim 0.1 M_{\odot}$ (luminous super-Chandrasekhar mass SNe Ia), producing hydrogen lines in a later phase as shown in Leonard (2007).

As for the fourth (last) point, which is the theme of this paper, we have already shown the possible cases where the WD mass increases up to $\sim 2.4 M_{\odot}$ based on our SD scenario. Thus, we are able to resolve the four major arguments raised by Howell (2011) against the SD scenario.

5.3. Young Progenitors in Low Metallicity Environments

Our calculations show that super-Chandrasekhar mass SNe Ia come preferentially from a pair of a massive C+O WD ($\gtrsim 1 M_{\odot}$) and a $4\text{--}5 M_{\odot}$ main-sequence star, thus indicating a rather younger population than several hundred Myr or so. In Section 4.1, we further show that very luminous super-Chandrasekhar mass SNe Ia such as SN 2007if/SN 2009dc are preferentially born in low metallicity environment because more massive initial C+O WDs ($\sim 1.1\text{--}1.2 M_{\odot}$) are required. Here we discuss these conditions in view of observational aspects.

Recent observation of the SN 2007if host galaxy suggests a low metallicity environment of $Z \sim Z_{\odot}/9\text{--}Z_{\odot}/5$ as well as a young population of the progenitor from the host galaxy turn-off mass of $M \sim 4.6^{+2.6}_{-1.4} M_{\odot}$ (Childress et al. 2011), which is consistent with our luminous super-Chandrasekhar mass model that can attain the maximum WD mass at $4\text{--}5 M_{\odot}$ in our binary evolutions (Figure 4). We could have super-Chandrasekhar mass models even in such a low metallicity environment. Although Kobayashi et al. (1998) showed that SNe Ia may not frequently occur in low metallicity environments (say, $Z \lesssim Z_{\odot}/10$) because optically thick winds are weak, we here point out that the metallicity of the SN 2007if host galaxy is still large enough for massive WDs (with the initial mass of $M_{\text{WD},0} = 1.1\text{--}1.2 M_{\odot}$) to blow strong winds (see Figure 1). Even for the metallicity of Population II ($Z = 0.001$), massive WDs ($M_{\text{WD},0} \geq 1.1 M_{\odot}$) can blow strong winds and, as a result, the stripping effect works. Thus, in such a low metallicity environment, we expect (super-Chandrasekhar mass) SN Ia explosions in our SD scenario.

Young population of the progenitor was also suggested for SN 2009dc. Taubenberger et al. (2011) suggested that UGC 10063 (suspected host galaxy of SN 2009dc if the supernova is in the edge of the tidal tail toward the galaxy UGC 10064) underwent a strong burst of star formation a few hundred Myr before the explosion of SN 2009dc (see also Figure 14 of Silverman et al. 2011, for images and position of UGC 10063, UGC 10064, and SN 2009dc). Our favorite model has an MS companion of mass $\sim 4\text{--}5 M_{\odot}$. A $4\text{--}5 M_{\odot}$ MS evolves to the end of central hydrogen burning a few hundred Myr after its born. Thus our model is consistent with these circumstances.

From these observational aspects, we may propose that luminous super-Chandrasekhar mass SNe Ia come preferentially from a low metallicity environment. This is because the AGB wind (or superwind) is relatively weak for $Z \lesssim 0.002 \sim Z_{\odot}/10$ so that the C+O WD can grow up to $\sim 1.2 M_{\odot}$ before the first common envelope evolution. On the other hand, the WD accretion (optically thick) wind is still strong enough for a $\sim 1.2 M_{\odot}$ WD, if the metallicity is larger than $Z \gtrsim 0.0002 \sim Z_{\odot}/100$. Considering these rare circumstances (a narrow range of WD masses and a low metallicity environment), we expect rather rare events of super-Chandrasekhar

mass SNe Ia.

6. CONCLUSIONS

Recent observations of Type Ia supernovae (SNe Ia) suggest that some of the progenitor white dwarfs (WDs) had masses up to $2.4\text{--}2.8 M_{\odot}$, which are highly exceeding the Chandrasekhar mass limit. Introducing three binary evolution processes into our binary evolution code, i.e., optically thick winds from mass-accreting WDs, mass-stripping from the binary companion star by the WD winds, and WDs being supported by differential rotation, we have calculated new SD evolutionary models of SN Ia progenitors and found following main results:

1. Since the mass-stripping attenuates the mass transfer from the companion to the WD, which prevents a binary even with a massive main-sequence companion of $\sim 4\text{--}5 M_{\odot}$ from being merged. As a result, the WD mass can increase by accretion up to 2.3 (2.7) M_{\odot} from the initial value of 1.1 (1.2) M_{\odot} . The newly obtained results satisfy the requirements of recent high luminosity SNe Ia such as SN 2007if and SN 2009dc.

2. There are three characteristic mass ranges of exploding WDs depending on the secular instability and rotation law: (i) $M_{\text{WD}} > 2.4 M_{\odot}$ triggered by a secular instability at $T/|W| = 0.14$, (ii) $M_{\text{WD}} = 1.5\text{--}2.4 M_{\odot}$ supported by differential rotation, and (iii) $M_{\text{WD}} = 1.38\text{--}1.5 M_{\odot}$ supported by rigid rotation. These three cases are explained as follows:

3. If the initial C+O WD is as massive as $\sim 1.1\text{--}1.2 M_{\odot}$, $T/|W|$ exceeds 0.14 when the WD mass reaches $M_{\text{WD}} \approx$

$2.4 M_{\odot}$. We expect an SN Ia explosion soon after a secular instability sets in at $M_{\text{WD}} \approx 2.4 M_{\odot}$. We regard that this kind of binary evolution corresponds to very luminous super-Chandrasekhar mass SNe Ia such as SN 2007if/SN 2009dc. These SNe Ia must be young (younger than a few hundred Myr).

4. If the initial C+O WD mass is $\sim 0.9\text{--}1.1 M_{\odot}$, $T/|W|$ does not exceed 0.14 before \dot{M}_1 becomes smaller than $\dot{M}_b = 3 \times 10^{-7} M_{\odot} \text{ yr}^{-1}$, where we stop our binary evolution. Loss or redistribution of angular momentum leads to an increase in the central density until carbon is ignited to induce the WD explosion as an SN Ia. This waiting time for an SN Ia depends entirely on the timescale of angular momentum loss/redistribution. It is shorter than $10^8\text{--}10^9$ yr (angular momentum redistribution by the Eddington-Sweet circulation in WDs). Therefore we suggest that these SNe Ia are relatively young, and correspond to the ‘‘prompt’’ component.

5. If the initial C+O WD mass is $\sim 0.7\text{--}0.8 M_{\odot}$, it reaches $M_{\text{WD}} \approx 1.38\text{--}1.5 M_{\odot}$, which can be supported by rigid rotation.

This research has been supported in part by the Grant-in-Aid for Scientific Research of the Japan Society for the Promotion of Science (20540227, 22012003, 22540254, 23105705, 23540262) and by World Premier International Research Center Initiative, MEXT, Japan.

REFERENCES

- Belczynski, K., & Mikołajewska, J. 1998, MNRAS, 296, 77
 Bianco, F. B. et al. 2011, ApJ, submitted (arXiv:1106.4008)
 Blöcker, T. 1995, A&A, 297, 727
 Bowen, G. H., & Willson, L. A. 1991, ApJ, 375, L53
 Brandi, E., Quiroga, C., Mikołajewska, J., Ferrer, O. E., & Garca, L. G. 2009, A&A, 497, 815
 Chandrasekhar, S. 1939, An introduction to the study of stellar structure (University of Chicago Press, Chicago), Chap. 11
 Chen, W.-C., & Li, X.-D. 2009, ApJ, 702, 686
 Childress, N., et al. 2011, ApJ, 733:3
 de Beck, E., Decin, L., de Koter, A., Justtanont, K., Verhoelst, T., Kemper, F., & Menten, K. M. 2010, A&A, 523, A18
 de Marco, O., Passy, J.-C., Moe, M., Herwig, F., Mac Low, M.-M., & Paxton, B. 2011, MNRAS, 411, 2277
 Di Stefano, R., Voss, R., & Claeys, J. S. W. 2011, ApJ, in press (arXiv:1102.4342)
 Frogel, J. A., & Whitelock, P. A. 1998, AJ, 116, 754
 Fujimoto, M. Y. 1993, ApJ, 419, 768
 Ganeshalingam, M., Li, W., & Filippenko, A. V. 2011, MNRAS, in press (arXiv:1107.2404)
 Gilfanov, M., & Bogdán, A. 2010, Nature, 463, 924
 Hachisu, I. 1986, ApJS, 61, 479
 Hachisu, I., & Kato, M. 2001, ApJ, 558, 323
 Hachisu, I., & Kato, M. 2003a, ApJ, 590, 445
 Hachisu, I., & Kato, M. 2003b, ApJ, 598, 527
 Hachisu, I., Kato, M., Kato, T., & Matsumoto, K. 2000a, ApJ, 528, L97
 Hachisu, I., Kato, M., & Nomoto, K. 1996, ApJ, 470, L97
 Hachisu, I., Kato, M., & Nomoto, K. 1999a, ApJ, 522, 487
 Hachisu, I., Kato, M., & Nomoto, K. 2008a, ApJ, 679, 1390
 Hachisu, I., Kato, M., & Nomoto, K. 2008b, ApJ, 683, L127
 Hachisu, I., Kato, M., & Nomoto, K. 2010, ApJ, 724, L212
 Hachisu, I., Kato, M., Nomoto, K., & Umeda, H. 1999b, ApJ, 519, 314
 Hayden, B. T. et al. 2010, ApJ, 722, 1691
 Herwig, F. 2005, ARA&A, 43, 435
 Hicken, M., Garnavich, P. M., Prieto, J. L., Blondin, S., DePoy, D. L., Kirshner, R. P., & Parrent, J. 2007, ApJ, 669, L17
 Hillebrandt, W., Sim, S. A., & Röpke, F. K. 2007, A&A, 465, L17
 Howell, D. A. 2011, Nature Communications, 2, 350 (arXiv:1011.0441)
 Howell, D., et al. 2006, Nature, 443, 308
 Iglesias, C. A. & Rogers R. J., 1996, ApJ, 464, 943
 Ilkov, M., & Soker, N. 2011, MNRAS, in press (arXiv:1106.2027)
 Justham, S. 2011, ApJ, 30, L34
 Khan, R., Stanek, K. Z., Stoll, R., & Prieto, J. L. 2011, ApJ, submitted (arXiv:1106.3071)
 Kasen, D. 2010, ApJ, 708, 1025
 Kato, M., & Hachisu, I. 1994, ApJ, 437, 802
 Karakas, A. I. 2010, MNRAS, 403, 1413
 Kawai, Y., Saio, H., & Nomoto, K. 1988, ApJ, 328, 207
 Kobayashi, C., Tsujimoto, T., Nomoto, K., Hachisu, I., & Kato, M. 1998, ApJ, 503, L155
 Langer, N., Deutschmann, A., Wellstein, S., & Höflich, P. 2000, A&A, 362, 1046
 Leonard, D. C. 2007, ApJ, 670, 1275
 Lindblom, L. 1999, Physical Review D, 60, 064007
 Liu, W.-M.; Chen, W.-C.; Wang, B.; Han, Z. W. 2010, A&A, 523, A3
 Marietta, E., Burrows, A., & Fryxell, B. 2000, ApJS, 128, 615
 Magrini, L., et al. 2003, A&A, 407, 51
 Mereghetti, S., La Palombara, N., Tiengo, A., Pizzolato, F., Esposito, P., Woudt, P. A., Israel, G. L., & Stella, L. 2011, ApJ, in press (arXiv:1105.6227)
 Niemeyer, J., & Hillebrandt, W. 2004, A&A
 Nomoto, K. 1982a, ApJ, 253, 798
 Nomoto, K., & Kondo, Y. 1991, ApJ, 367, L19
 Nomoto, K., Saio, H., Kato, M., & Hachisu, I. 2007, ApJ, 663, 1269
 Nomoto, K., Umeda, H., Kobayashi, C., Hachisu, I., Kato, M., & Tsujimoto, T. 2000, in AIP Conf. Proc. Vol. 522: Cosmic Explosions: Tenth Astrophysics Conference, ed. S. S. Holt & W. W. Zhang (American Institute of Physics), 35 (astro-ph/0003134)
 Paczynski, B. 1991, ApJ, 370, 597
 Panagia, N., Van Dyk, S. D., Weiler, K. W., Sramek, R. A., Stockdale, C. J., Murata, K. P. 2006, ApJ, 646, 369 (Erratum: 2011, ApJ, 733, 72)
 Patat, F. et al. 2007, Science, 317, 924
 Pfannes, J. M. M., Niemeyer, J. C., & Schmidt, W. 2010, A&A, 509, A75
 Piersanti, L., Gagliardi, S., Iben, I. Jr., Tornambé, A. 2003a, ApJ, 583, 885
 Piersanti, L., Gagliardi, S., Iben, I. Jr., Tornambé, A. 2003b, ApJ, 598, 1229
 Popham, R., & Narayan, R. 1991, ApJ, 370, 604
 Piro, A. L. 2008, ApJ, 679, 616
 Saio, H., & Nomoto, K. 1998, ApJ, 500, 388

- Saio, H., & Nomoto, K. 2004, *ApJ*, 615, 444
Saio, H., Nomoto, K., & Kato, M. 1988, *ApJ*, 331, 388
Scalzo, R. A., et al. 2010, *ApJ*, 713, 1073
Siess, L. 2010, *A&A*, 512, A10
Silverman, J. M., Ganeshalingam, M., Li, W., Filippenko, A. V., Miller, A. A., & Poznanski, D. 2011, *MNRAS*, 410, 585
Steinmetz, M., Müller, E., & Hillebrandt, W. 1992, *A&A*, 254, 177
Tanaka, M., et al. 2010, *ApJ*, 714, 1209
Taubenberger, S., et al. 2011, *MNRAS*, 412, 2735
Thoroughgood, T. D., Dhillon, V. S., Littlefair, S. P., Marsh, T. R., & Smith, D. A. 2001, *MNRAS*, 327, 1323
Uenishi, T., Nomoto, K., & Hachisu, I. 2003, *ApJ*, 595, 1094
Umeda, H., Nomoto, K., Yamaoka, H., & Wanajo, S. 1999, *ApJ*, 513, 861
Vassiliadis, E., & Wood, P. R. 1993, *ApJ*, 413, 641
Ventura, P., & D'Antona, F. 2009, *A&A*, 499, 835
Ventura, P., & D'Antona, F. 2011, *MNRAS*, 410, 2760
Wang, B., & Han, Z.-W. 2010, *Research in Astronomy and Astrophysics*, 10, 681
Webbink, R. F. 2007, in *Short-Period Binary Stars: Observations, Analyses, and Results*, ed. E. F. Milone, D. A. Leahy, and D. W. Hobill (Springer, Berlin), 233
Weidemann, V. 2000, *A&A*, 363, 647
Weiss, A., & Ferguson, J. W. 2009, *A&A*, 508, 1343
Yamanaka, M., et al. 2009, *ApJ*, 707, L118
Yoon, S.-C., & Langer, N. 2004, *A&A*, 419, 623
Yoon, S.-C., & Langer, N. 2005, *A&A*, 435, 967
Zijlstra, A. A. 2004, *MNRAS*, 348, L23